Directional Validation of Wave Predictions*

W. ERICK ROGERS AND DAVID W. C. WANG

Oceanography Division, Naval Research Laboratory, Stennis Space Center, Mississippi

(Manuscript received 28 April 2005, in final form 15 May 2006)

ABSTRACT

A methodology for quantitative, directional validation of a long-term wave model hindcast is described and applied. Buoy observations are used as ground truth and the method does not require the application of a parametric model or data-adaptive method to the observations. Four frequency ranges, relative to the peak frequency, are considered. The validation of the hindcast does not suggest any systematic bias in predictions of directional spreading at or above the spectral peak. Idealized simulations are presented to aid in the interpretation of results.

1. Introduction

a. Background

1) IMPORTANCE/RELEVANCE

Principal wave direction, quantified as a mean or peak value, is of obvious importance to wave prediction. Directional distribution about the mean or peak direction is also very important for wave modeling. It can have a large impact on the prediction of swells, since it determines how far and wide the swells will disperse. Nonlinear interactions computed by a wave model are sensitive to the directional distribution of energy. Further, as wave model dissipation terms with more sophisticated directional dependency are developed, we can expect that directional spreading will have greater influence on the modeled source term balance and, thus, total energy.

2) PRESENT CAPABILITY

Validations of modeled peak or mean wave direction in the literature typically show good skill, though the response of a third-generation wave model to rapidly turning winds is a concern (e.g., Young et al. 1987). The ability of third-generation models to accurately predict the width of the directional distribution is poorly understood. Indeed, as is described in a companion manuscript (Rogers and Wang 2006, hereafter RW), evaluations in the literature show very little consensus.

b. Model description

The so-called third-generation (3G) of spectral wave models calculate wave spectra without a priori assumptions regarding spectral shape. For this investigation, we use the Simulating Waves Nearshore model (SWAN; Booij et al. 1999). SWAN is a 3G model designed to address the excessive computational expense of applying predecessor 3G models (such as WAM; WAMDI Group 1988) in coastal regions. The governing equation of SWAN and most other 3G wave models is the action balance equation. In Cartesian coordinates, the action balance equation is

$$\frac{\partial N}{\partial t} + \frac{\partial C_{g,x} N}{\partial x} + \frac{\partial C_{g,y} N}{\partial y} + \frac{\partial C_{g,\sigma} N}{\partial \sigma} + \frac{\partial C_{g,\theta} N}{\partial \theta} = \frac{S}{\sigma},$$

where σ is the relative frequency, which is the wave frequency measured from a frame of reference moving with a current, if a current exists; N is the wave action density, equal to the energy density divided by the relative frequency ($N = E/\sigma$); θ is the wave direction; C_g is the wave action propagation speed in (x, y, σ, θ) space; and S is the total of source–sink terms expressed as wave energy density. In deep water, the right-hand side

* Naval Research Laboratory Contribution Number NRL/JA/7320-05-5179.

Corresponding author address: W. Erick Rogers, Oceanography Division, Naval Research Laboratory, Code 7320, Stennis Space Center, MS 39529.
E-mail: rogers@nrlssc.navy.mil

DOI: 10.1175/JTECH1990.1

of the governing equation is dominated by three terms: $S \approx S_{in} + S_{nl} + S_{ds}$ (input by wind, four wave nonlinear interactions, and dissipation, respectively). These three deepwater source–sink terms are discussed at several points later in this manuscript. SWAN also includes physical processes associated with intermediate-depth and shallow water (e.g., bottom friction, depth-limited breaking).

c. Objective

It has become increasingly common for a wave modeler to have at his or her disposal directional wave observations within a model computational domain. This often leads to an expectation—perhaps a naïve expectation—that the wave modeler can readily use these observations to validate the model. Unfortunately, validating a model using directional observations is much less straightforward than traditional validations of wave height or peak period. For example, what if the model in question is a long-term simulation with continuous directional observations? How could one perform a meaningful validation that is compact enough to be presented to others? How far can one go in condensing these comparisons? At what point do the comparisons become meaningless or misleading?

This study was initiated with three general objectives: 1) to review the history and state of the art for directional wave validation methods, 2) to design a validation methodology/strategy best suited for a specific model application, and 3) to characterize model behavior in that specific application. The first general objective is addressed only briefly in this manuscript; a companion manuscript (RW) provides a more detailed review. The specifics of the second and third general objectives are given here.

1) REQUIREMENTS ON VALIDATION DESIGN

The major challenge of this study is in the design of a validation method. Since we are allowed the luxury here of focusing primarily on directional wave validation, we were not satisfied with the simplest and most obvious method, which is to use buoy data and a parametric model or data-adaptive method to create directional spectra, and make qualitative side-by-side comparisons with model directional spectra at a few instants in time. Rather, we have fairly specific self-imposed requirements on the validation method.

The first requirement is that it be a *long-term* directional validation, without extensive manipulation of the output, for example to isolate the pure windsea events. Usually, when directional spreading *is* a primary focus, the investigators focus on specific events. This leads to uncertainties with regard to generality: is a conclusion specific to the event, or is it a systematic symptom of the model physics? We address this limitation using a relatively long simulation.

The second requirement is to develop and employ a method of evaluation of model directional skill that is *quantitative*, in other words a comparison of model and observation value pairings from which statistics may be calculated; traditionally, this is presented as a scatterplot comparison of modeled and observed values. Since many comparisons in the literature are short-term comparisons, it is possible to simply present modeled and observed two-dimensional spectra side by side, thereby avoiding the necessity of condensing results. With long-term simulations, it is necessary to condense results somehow.

The third requirement is that the method of evaluation of model directional skill also *utilizes observational data as they are given,* rather than applying a parametric model [e.g., the well-known $\cos^{2s}$ model; Longuet-Higgins et al. 1963); Cartwright (1963)] or a data-adaptive method. Two popular methods are the maximum likelihood estimator [referred to as MLE or MLM; Capon et al. (1967) and Oltman-Shay and Guza (1984)] and the maximum entropy method (MEM; Lygre and Krogstad 1986) to transform the observational data into a *subjective* directional spectrum. For discussion and a description of this subjectivity, we refer the reader to Kuik et al. (1988) and Benoit et al. (1997).

Our fourth requirement is that the observational data be taken from a buoy. Other data sources, such as radar, have been used with success in the past for directional validation, but these datasets tend to have more limited availability or accessibility.

Our fifth requirement is that the frequency variation of directional spreading be considered, as opposed to a quantity integrated from the entire frequency range.

2) MODEL CHARACTERIZATION

The objective is to quantitatively determine whether a typical 3G model (SWAN; Booij et al. 1999), in a typical implementation, has a systematic tendency to overpredict or underpredict directional spreading. The Discrete Interaction Approximation (DIA) for four-wave nonlinear interactions, S_{nl4}, is the approximation used by all operational 3G wave models today. It is has been demonstrated a number of times in the literature that this approximation leads to broader directional spreading than would be obtained with more rigorous calculations (Hasselmann et al. 1985; Young et al. 1987; Young and Van Vledder 1993; Cardone and Resio 1998; Forristall and Ewans 1998, etc.). This can result in

TABLE 1. Summary of notation.

f	Frequency, T^{-1}
σ	The relative (intrinsic) radial frequency, $2\pi T^{-1}$
θ	Direction of wave propagation
$\sigma_\theta(f)$	The rms circular spreading (note, σ here is unrelated to frequency)
$\overline{\sigma}_\theta$	Mean rms circular spreading; "mean" here refers to some integration over frequencies
N	Two-dimensional spectral wave action density, $N(f, \theta)$
E	Two-dimensional spectral variance density, $E(f, \theta)$
F	One-dimensional spectral variance density, $F(f)$
$D(\theta)$	Dimensionless directional distribution at a particular frequency; integrates to unity
f_1 and f_2	Lower and upper bounds of a frequency integration
$\theta_0(f)$	Mean wave direction, taken as the circular centroid of $D(\theta)$, and denoted $\alpha_1(f)$ in NDBC notation
$\theta_p(f)$	Peak wave direction, the peak of $D(\theta)$; generally not known, except in the context of a model of some sort
$\overline{\theta}_0$	Mean–mean wave direction, which has been integrated across some frequency range
$m_1(f)$	Parameter related to directional spreading, denoted r_1 in NDBC notation
a_1, b_1, a_2, b_2	Fourier coefficients

an expectation that 3G wave models systematically overpredict directional spreading. This is sometimes observed in the literature, but the reverse has also been found (Jensen et al. 1995). One wonders how much this "expectation" has influenced prior comparisons. Long-term comparisons can be used to convincingly argue for or against this broadening effect. We know from the literature that in cases of pure windsea, directional spreading tends to follow a fairly consistent pattern relative to the peak frequency: directional spreading at the peak is relatively narrow, and spreading is broader farther from (higher and lower than) the peak. A secondary objective is to verify that an operationally used wave model (SWAN with the DIA approximation for four-wave interactions) adequately reproduces this pattern in directional spreading.

3) PRIOR WORKS

A number of methods for directional validation of wave predictions have been applied over the years. Due to page limits, a detailed review of this prior work is described separately (RW). There have been no prior works that fit the five requirements described above. There have, of course, been a number of studies that share some similarities. For example, Komen et al. (1994, chapter V.4), Khandekar et al. (1994), and Forristall and Greenwood (1998) describe the validation of directional spreading of hindcasts of medium (15 days) or longer duration. Jensen et al. (1995), Forristall and Greenwood (1998), Ardhuin et al. (2003), and Wyatt et al. (2003) all include quantitative non-data-adaptive comparisons for validation of hindcast directional spreading with in situ data as ground truth. Forristall et al. (1978), Komen et al. (1984), Tolman (1991), Forristall and Ewans (1998), Forristall and Greenwood (1998), and Alves and Banner (2003) include quantitative validations of directional spreading, with some description of the variation with frequency. Of these, only Forristall et al. (1978) was a hindcast of a specific event, as opposed to an idealized simulation, and showed the frequency variation simply by choosing a few specific instances in time. For further descriptions of prior work on the subjects of directional metrics, directional model validation, and parametric directional distributions, we refer the reader to RW.

d. Terminology

The two-dimensional energy density spectrum is defined as $E(f, \theta) = D(f, \theta)F(f)$, where $D(f, \theta)$ is the normalized directional distribution and $F(f)$ is the one-dimensional energy density spectrum. The function $D(f, \theta)$ is normalized such that $\int_0^{2\pi} D(f, \theta)d\theta = 1$.

"Directional spreading" refers to the degree to which a directional distribution of wave energy is "broad." It does not refer to the normalized directional distribution itself, which is sometimes referred to as the "directional spreading function." Notations used herein are given in Table 1.

e. Organization of manuscript

In section 2, the methodology of this study (general validation strategy and definition of metrics used) is described. In section 3, an idealized case is examined to isolate the effect of the inaccuracy of the Discrete Inter-Action approximation for four-wave nonlinear interactions. In section 4, an example directional validation is presented for a hindcast with the SWAN model in Lake Michigan during fall 2002. Results are summarized in section 5. Discussion is given in section 6 and conclusions in section 7.

2. Method

a. General strategy

1) GROUND TRUTH

Buoy data are the "ground truth" of this study—specifically, National Data Buoy Center (NDBC) buoy 45007 in Lake Michigan. Directional buoys are often the most cost-effective method of obtaining directional data outside the surf zone. [In depths shallower than around 150 m, three-element pressure gauge arrays and p–u–v gauges can be cost-effective methods of obtaining information that is essentially the same as that from a heave-pitch-roll buoy. Additional elements in a pressure gauge or wave staff array will yield higher-resolution directional data; see Young (1994).]

2) NONDIRECTIONAL ACCURACY

We aim to perform a model validation in which directional characteristics are the *primary* focus. Usually, when directional metrics are used in validation, they are secondary, with the primary focus being wave height, wave period, and—more rarely—frequency spectra. Here, we want to devote most of our attention to the directional issue. We do this by taking a modeling system that has consistently good skill with regard to nondirectional metrics.

3) CHALLENGE: PROBLEM COMPLEXITY

Our objective is to determine the feasibility of conducting a *quantitative* directional validation of a long-term hindcast. Anticipating that is a major challenge even under the most favorable circumstances; we simplify our case study by taking the following steps.

1) We use a lake as our test basin (Lake Michigan, Fig. 1); thus, the wave climate is dominated by windsea. Mixed sea/swell states (identifiable as having multiple peaks) do occur (especially when the wind shifts rapidly), but are uncommon. Certainly, old swells do not occur.
2) We use a model (SWAN) that has proven to be skillful in predicting nondirectional spectra at this scale, in wind sea-dominated cases (Rogers et al. 2003).
3) We make comparisons at only one location (at the location of buoy 45007 in Fig. 1).
4) For model–data comparisons, we use a location near the center of the lake. The depth is 165 m, which is relatively deep water for the typical wave frequencies in the lake. Thus, the impact of finite depth physics is limited.

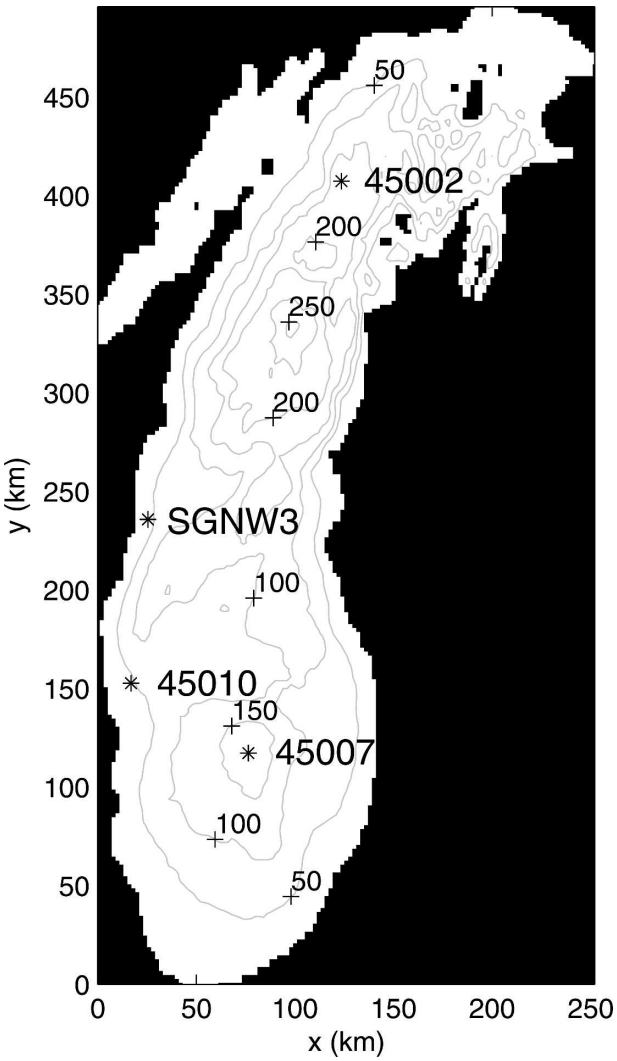

FIG. 1. Lake Michigan, with depth contours (m) and NDBC instrument locations shown.

4) CHALLENGE: DESCRIBING FREQUENCY VARIATION

The primary challenge with quantitative directional validation of a long time series is that a different set of low-order moments exists for every frequency band. That is one dimension. Combine that with the time dimension, and the validation quickly becomes unmanageable. One can make a qualitative comparison by plotting these moments as a function of time and frequency, but our objective is to make quantitative comparisons. Thus, it is necessary to perform some kind of integration in frequency space. Yet we cannot throw out the frequency-wise variation of these moments altogether, since (as was mentioned in section 1) one objective of this study is to determine whether an operationally used wave model adequately reproduces the directional spreading as a function of frequency relative

to the spectral peak. Thus, there are two competing motivators: 1) the desire to make the problem more manageable via frequency-wise integration of directional metrics and 2) the desire to describe the frequency-wise variation in directional spreading.

Our approach is a compromise between these two motivators. We retain frequency-wise bins, but use fewer bins than are used in the model computational grid:

1) 0.5–0.8 times the relative frequency f/f_p ("low frequencies"),
2) $0.8f/f_p$–$1.2f/f_p$ ("frequencies at and near the peak"),
3) $1.2f/f_p$–$2.0f/f_p$ ("frequencies above the peak"), and
4) $2.0f/f_p$–$3.0f/f_p$ ("highest frequencies").

5) Challenge: Defining the peak frequency

To quantify the variation of the directional spreading as a function of relative frequency, it is obviously necessary to define the peak frequency. Though this may sound simple, it is subject to problems, since even in a region like Lake Michigan, with its typically simple sea states, peak frequency can be a rather unstable quantity, with significant model–data mismatch being not uncommon. Obviously, it is very problematic to compare *model directional spreading as a function of modeled relative frequency* to *observed directional spreading as a function of observed relative frequency* in cases where the modeled and observed peak frequencies are very dissimilar. Model predictions of mean period tend to be more reliable and much more stable. To address this, we use a "synthetic peak period," which is a simple function of the mean period. The relation is determined using a simple linear regression of the two metrics for the time period of the hindcast described in section 5 below. The mean period is calculated over the frequency range of 0.07–0.4 Hz. For the modeled values, the result of the regression is

$$T_p = 1.2142T_{\text{mean}} - 0.7126.$$

For the buoy, the regression is

$$T_p = 1.2325T_{\text{mean}} - 0.7051.$$

In subsequent discussions, T_p and f_p refer to this synthetic peak period *except* in one case where it is explicitly stated that the "true" peak period is presented.

6) Challenge: Avoiding parametric models and data-adaptive methods

It was mentioned in section 1 that one objective is to avoid using a parametric model (e.g., the $\cos^{2s}$ model) or a data-adaptive method (e.g., MLE and MEM) to infer directional characteristics from the buoy data. The solution is simply to use only variables directly extracted from what the buoy measures: we transform the model to yield quantities analogous to what the buoy measures. This approach has been taken by others; for example, Ardhuin et al. (2003). The specific calculations are described in section 2b.

b. Definition of directional metrics

There exists a separate directional distribution function for each frequency component that can be decomposed into a Fourier series:

$$D(f, \theta) = \frac{1}{\pi}\left\{\frac{1}{2} + \sum_{n=1}^{\infty} [a_n \cos(n\theta) + b_n \sin(n\theta)]\right\}, \tag{1}$$

where

$$a_n(f) = \int_0^{2\pi} D(f, \theta) \cos n\theta \, d\theta \quad \text{and} \tag{2}$$

$$b_n(f) = \int_0^{2\pi} D(f, \theta) \sin n\theta \, d\theta.$$

The first four Fourier coefficients (a_1, b_1, a_2, b_2) can be inferred from the signals measured by a heave–pitch–roll directional buoy. This permits only an approximation from the truncated Fourier series (Longuet-Higgins et al. 1963; Kuik et al. 1988), which is

$$D^*(f, \theta) = \frac{1}{\pi}\left\{\frac{1}{2} + \sum_{n=1}^{2} [a_n(f) \cos(n\theta) + b_n(f) \sin(n\theta)]\right\} \tag{3}$$

Unfortunately, Eq. (3) has limited utility for describing $D(f, \theta)$, since it is only accurate if the unmeasured, higher-order Fourier components are very small. One possible manifestation of this inaccuracy is negative values of $D^*(f, \theta)$. Parametric models (such as the $\cos^{2s}$ form) have been developed to yield more natural (and thus presumably more accurate) representations of $D(f, \theta)$ given the measured low-order moments, but these models give details of $D(f, \theta)$ that are not actually determinable from buoy motion. Further, at least one commonly used data-adaptive method—the maximum likelihood estimator—produces a $D(f, \theta)$ that is inconsistent with the original cross-spectral matrix elements (Oltman-Shay and Guza 1984). Kuik et al. (1988) suggest "model free" expressions for mean wave direction θ_0 and directional width σ_θ. Kuik et al. also suggested two higher-order statistics (skewness and kurtosis) that

we do not use herein. All four statistics are expressible as functions of the four Fourier coefficients $[a_1(f), b_1(f), a_2(f), b_2(f)]$. Mean wave direction is given as $\theta_0(f) = \arctan[b_1(f)/a_1(f)]$. Directional width is quantified as the "circular RMS spreading":

$$\sigma_\theta(f) = \sqrt{2[1 - m_1(f)]}, \tag{4}$$

where $m_1(f) = \sqrt{a_1(f)^2 + b_1(f)^2}$.

The calculation in reverse is $a_1 = m_1 \cos\theta_0$ and $b_1 = m_1 \sin\theta_0$.

Real-time and historical data from directional National Data Buoy Center (NDBC) buoys include estimates of the low-order moments θ_0 and m_1 (Steele et al. 1985).[1] We will first discuss in detail the calculation of the mean direction and then do the same for the directional spreading.

CALCULATION OF MEAN WAVE DIRECTION AND DIRECTIONAL SPREADING

In the literature, the mean direction is the most commonly presented directional property of waves (e.g., in maps of wave heights with arrows representing mean direction). Models such as SWAN (Booij et al. 1999) and WAVEWATCH-III (WW3; Tolman 1991, 2002) directly calculate actual two-dimensional spectra $E(f)$, θ) and output-averaged θ_0 for frequencies f_1–f_2 calculated as

$$\overline{\theta}_0 = \arctan\left(\frac{\overline{b}_1}{\overline{a}_1}\right), \tag{5}$$

where

$$\overline{a}_1 = \int_0^{2\pi}\int_{f_1}^{f_2} E(f,\theta)\cos\theta\, df\, d\theta/\overline{E} \quad \text{and}$$

$$\overline{b}_1 = \int_0^{2\pi}\int_{f_1}^{f_2} E(f,\theta)\sin\theta\, df\, d\theta/\overline{E}, \tag{6}$$

where $\overline{E} = \int_0^{2\pi}\int_{f_1}^{f_2} E(f,\ \theta)dfd\theta$. (SWAN and WW3 are coded to output $\overline{\theta}_0$ only for f_1 and f_2 equal to 0 and ∞, respectively.)

Now, we want to derive $\overline{\theta}_0$ based on a_1, b_1 from the buoy's measurements according to the SWAN–WW3 definition in (5). We use

$$\overline{a}_1 = \int_{f_1}^{f_2} a_1(f)F(f)\, df/\overline{E} \quad \text{and}$$

$$\overline{b}_1 = \int_{f_1}^{f_2} b_1(f)F(f)\, df/\overline{E}, \tag{7}$$

$$\text{where } \overline{E} = \int_{f_1}^{f_2} F(f)\, df.$$

Note that if we choose f_1 and f_2 as values close to f_p, say $f_1 = 0.9f_p$ and $f_2 = 1.1f_p$, this is in practice very similar to the "mean wave direction corresponding to energy of the dominant period" (MWD) reported by NDBC and to the "D_p" reported by the Coastal Data Information Program (CDIP) ("mean direction from which energy is coming at the peak period"). The use of a broader band of frequencies makes the metric more stable, but increases the risk that two distinct wave systems could be integrated together.

As with mean direction, the directional spreading $\sigma_\theta = \sigma_\theta(f)$. In this study, we use a weighted mean of σ_θ over particular frequency ranges. We denote this as $\overline{\sigma}_\theta$. To be consistent with our calculation of mean direction (5), and with calculation methods of SWAN and WW3, the form of the calculation of the mean directional spread adopted in this paper is

$$\overline{\sigma}_\theta = \{2[1 - (\overline{a}_1{}^2 + \overline{b}_1{}^2)^{1/2}]\}^{1/2} \tag{8}$$

(WW3 uses $f_1 = 0$ and $f_2 = \infty$).

With the model, $\overline{a}_1$ and $\overline{b}_1$ are calculated as in (6). For buoy measurements, $\overline{a}_1$ and $\overline{b}_1$ are calculated as in (7).

3. An idealized case

Rather than move straight to the hindcast simulation, we will first provide an idealized application, since the idealized application is used as a point of discussion when interpreting the hindcast results.

a. Introduction of nonlinear interaction computation methods

One limitation of the dynamics used by third-generation (3G) wave models is the highly simplified DIA (Hasselmann et al. 1985) used to compute four-wave nonlinear interactions in both models: the DIA uses only a small subset of the possible resonant quadruplets. A software routine based on the Webb–Resio–Tracy method (WRT; see Resio and Perrie 1991 and references therein) has been implemented in the SWAN model by G. van Vledder, designated as "Xnl" in the user's manual. In contrast to the DIA, this

[1] *On notation used elsewhere*: NDBC uses the notation "α_1" instead of "θ_0" (used by Kuik et al. and herein) and "r_1" instead of "m_1" (used by Kuik et al. and herein). Further, the NDBC definitions of the Fourier coefficients (a_1, b_1, a_2, b_2) [as used in their literature such as Steele et al. (1985)] are dimensional, whereas we use the Kuik convention of nondimensional Fourier coefficients (a_1, b_1, a_2, b_2). The notation "α_1" is useful, as it indicates a relation to (a_1, b_1).

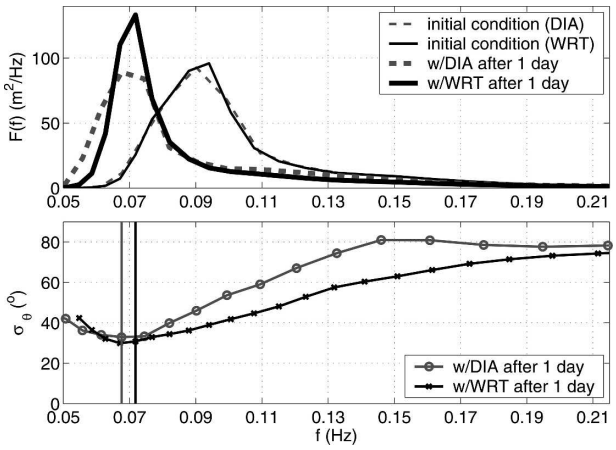

FIG. 2. Nondirectional spectral density distributions for the idealized simulations and circular rms spreading for the simulations with $S = S_{nl4}$. The vertical lines in the bottom panel indicate the peak frequencies of each model.

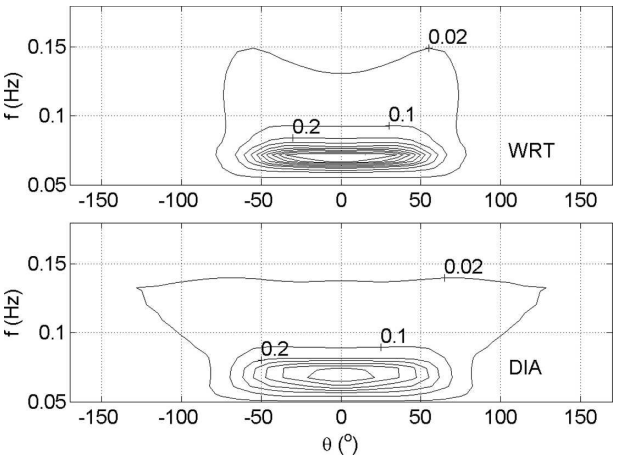

FIG. 3. Directional spectral density distributions for the $S = S_{nl4}$ idealized simulations: (top) the WRT (Xnl) and (bottom) the DIA results.

method is essentially exact, but relatively time consuming.

b. Simulation descriptions

An example application of this WRT subroutine is shown in Fig. 2. The computation is with a "point model," implying either zero propagation or infinite fetch: $(\partial C_{g,x}N/\partial x) + (\partial C_{g,y}N/\partial y) = 0$. First, a "spinup" simulation was run using all three deepwater source terms [DIA for nonlinear interactions, Tolman and Chalikov (1996) for wind input and dissipation], a constant wind speed of $U_{10} = 18$ m s^{-1}, and a duration of 1 day. The resulting spectrum[2] was used to initialize two simulations that are identical except that one uses WRT and the other DIA. These two simulations, also of 1-day duration, include only nonlinear interactions, to lend insight regarding the effect of nonlinear interactions on swell as it leaves its source. To summarize, the following spectra are presented here:

1) the initial conditions for the other two simulations, which is the final condition of the spinup simulation, and which includes all three deepwater source–sink terms, $S = S_{in} + S_{ds} + S_{nl4}$;
2) the final condition of a simulation, which includes only four-wave interactions, $S = S_{nl4}$, calculated using the WRT routine; and
3) the final condition of a simulation, which includes only four-wave interaction, $S = S_{nl4}$, calculated using the DIA routine.

Note that since this model does not include propagation, dispersion of the swell is not represented. The effects of dispersion could be significant within 1 day, depending on the size of the storm; this dispersion would be expected to reduce wave steepness and therefore nonlinear interactions. The differences seen here between the DIA and WRT models are qualitatively consistent with computations of the nonlinear source term by Hasselmann et al. (1985; e.g., see their Fig. 7).

c. Discussion of results

Figure 2 shows the nondirectional spectral density of the three spectra (top panel) and the directional spreading of the second and third spectra (bottom panel). Since only three spectra are being presented with no time dimension, it is not necessary to integrate in frequency space, and the actual variation with frequency at the model resolution is shown. Skewness and kurtosis for the second and third spectra were also compared, but the comparisons were not noteworthy and are not presented here. The two-dimensional spectral density distributions for the simulations with $S = S_{nl4}$ are shown in Fig. 3. In this figure, both spectra have been normalized by 1.19 m^2 Hz^{-1} $^{\circ -1}$, which is the maximum of the third spectrum. Thus, the contours are labeled relative to the peak of the larger spectrum. The following observations can be made.

- Though it is not directly related to the subject matter of this study, the effect of the inaccuracy of the DIA

[2] The slight difference between the two initial conditions is due to the difference in frequency resolution for the two simulations; with the DIA method, a logarithmic distribution with $f_i = 1.1f_{i-1}$ is preferred and with the WRT method, a higher resolution is preferred; we use $f_i = 1.07f_{i-1}$ (48 frequency bins from 0.0418 to 1.0 Hz).

on frequency downshifting is seen clearly in the spectral density plot.
- The inaccuracy of the DIA is leading to slightly too narrow a directional distribution at the low frequencies, slightly too broad a distribution near the peak, and clearly too broad spectra above the peak, most noticeable beyond 0.1 Hz.
- The directional spectrum plot (Fig. 3) gives an immediate visual impression that directional spreading is much greater with the DIA model; this is reflected quantitatively in Fig. 2. However, the higher directional spreading is really apparent only in the lowest energy contour (2% of peak), at the higher frequencies.

4. A hindcast validation

a. Simulation description

The grid domain is shown in Fig. 1. The following settings/features were identical to those of Rogers et al. (2003).

- Cartesian coordinates were used, with grid spacing of 2 km.
- The lake bathymetry is provided by the National Oceanic and Atmospheric Administration (NOAA)/Great Lakes Environmental Research Laboratory.
- The directional resolution is 10°.
- The wind field is created using wind observations from the two open-water buoys in Lake Michigan (45002 and 45007), adjusted to 10-m elevation, with linear interpolation in the latitudes, and no variation in longitude.
- Default parameterizations for S_{in}, S_{ds}, and S_{nl4} are used, except that the power on the relative wavenumber [denoted n in Rogers et al. (2003)] is set to 2.0. (The default parameterizations in SWAN are that of WAM, cycle 3, sometimes referred to in the literature as "WAM3 physics.")

The following settings/features are different from those of Rogers et al. (2003).

- Season hindcast covers 0000 UTC 1 September–0500 UTC 14 November 2002.
- The frequency grid is logarithmic, with 29 frequencies from 0.07 to 1.0 Hz.
- Since 1 September 2002 was relatively calm, only a very short "ramp" time was needed (6 h), so the comparisons to the data start at 0600 UTC 1 September.
- A time step of 6 min is used.
- The version of SWAN used is 40.41A (Booij et al. 2005).

The physical parameterizations used are not tuned for this simulation or for this area; rather, they are the same as those used in the SWAN forecasting systems run at NRL for other areas.

b. Simulation results

The primary focus of the study is the accuracy of the predictions of directional spreading in the hindcast. However, results of any validation of directional spreading will be much more meaningful if it is first shown that the nondirectional spectra and the mean direction are well predicted. Thus, we present results other than the directional spreading before making the comparisons of directional spreading.

1) RESULTS: NONDIRECTIONAL SPECTRA AND MEAN WAVE DIRECTIONS

To provide a sense of the length of the simulation and how many events are being verified, a time series of zero-moment wave height H_{m0}, at buoy 45007, is shown in Fig. 4. These wave heights are also compared to data in scatterplot form, along with the mean period, the mean-mean wave direction, and the true peak period, in Fig. 5.[3] Statistics associated with the comparison are indicated in the plots. The wave height and mean period are for the frequency range 0.07–0.4 Hz (essentially the entire spectrum). The mean–mean wave direction is the mean wave direction integrated over 0.8 f_p–1.2f_p using (5), so it is a stable metric of the mean direction near the peak frequency. By the standards of a wave model that uses only wind forcing, the agreement is very good for all four metrics. The good prediction of the wave height and mean period suggests that the nondirectional wave spectra $F(f)$ are fairly well predicted. This provides confidence that the hindcast is suitable for detailed study of the accuracy of the prediction of the directional spreading. Some bias is evident in the prediction of the mean period, indicating a problem with overestimation of energy below the peak or underestimation of energy above the peak, or both.

Even with excellent agreement in the three nondirectional parameters, there can still be problems with the frequency width that are not revealed. Thus, we present in Fig. 6 time-collocated scatterplot comparisons of the energy level in the four frequency bands described in section 2, quantifying the bias and random

[3] In the case of the peak period, the density of occurrence is plotted rather than individual points, since discrete peak period values tend to overlay each other.

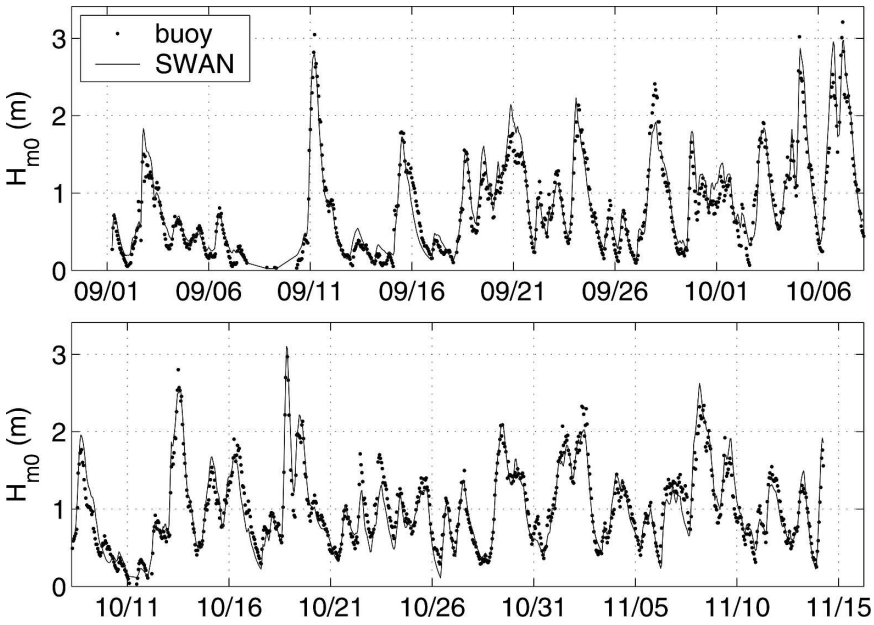

FIG. 4. Time series of zero-moment wave height (hindcast vs observation). Wave heights are calculated by integration of spectra from 0.07 to 0.4 Hz.

error in each band. The "partial wave height" presented in Fig. 6 is calculated from the variance (i.e., energy) of the wave spectrum over a frequency range defined by lower and upper bounds f_1 and f_2: $H_{m0,\text{partial}} = 4\sqrt{\upsilon_{\text{partial}}}$ and $\upsilon_{\text{partial}} = \int_{f_1}^{f_2} F(f)df$, the "partial variance." (The fictitious quantity $H_{m0,\text{partial}}$ is used rather than variance, since wave height is more intuitively understood.) A time-averaged nondirectional spectrum $F(f/f_p)$ is shown in Fig. 7. This is created by using 24 f/f_p bins instead of 4. Since it is time averaged, it quantifies bias only. The robust feature in Figs. 6 and 7 is an overestimation of energy below the spectral peak, thus explaining the modest positive bias in the mean period. Interestingly, the model–data comparison here is qualitatively very similar to the $F(f)$ comparison for the idealized case (Fig. 2, top panel). This similarity suggests that the overprediction of low-frequency energy in Fig. 7 is at least partially attributable to inaccuracy associated with the DIA. The problem can be compensated for by reducing the weighting on the relative wavenumber in the Komen et al. (1984) S_{ds} formulation used by SWAN, but this would only shift the positive bias to the frequencies *above* the peak: this has been verified by repeating the hindcast with a weighting of $n = 1.5$ instead of $n = 2.0$. [In SWAN, the default setting is $n = 1.0$, but this setting consistently leads to underprediction of the mean period in cases of wind speeds up to 21 m s^{-1}; for more detailed discussion of this tuning parameter in SWAN, see Rogers et al. (2003).]

In summary, low-frequency energy is overpredicted by the model in the hindcast (bias = 9 cm, $r = 0.64$), and this should be considered when evaluating directional spreading in this frequency range.

2) RESULTS: DIRECTIONAL SPREADING

(i) Scatterplot comparisons

The scatterplot comparisons of the mean directional spreading $\overline{\sigma}_\theta$ are made in Figs. 8a and 8b. Figure 8a is a simple scatterplot comparison of $\overline{\sigma}_\theta$; statistics associated with the comparison are shown in each plot. In Fig. 8b, the horizontal axis is the buoy partial wave height for the indicated frequency range, and the vertical axis is the misfit in the mean directional spreading, $\overline{\sigma}_{\theta,\text{hc}} - \overline{\sigma}_{\theta,\text{obs}}$. There are fewer points in the highest-frequency comparisons ($2f_p$ to $3f_p$) because the highest frequency in the directional buoy data is 0.35 Hz; thus, there are often no data available in this frequency range, depending on the value of f_p. In all plots of the directional spreading, "weak signal" data points are not included, being defined as collocated values for which either the buoy or modeled total wave heights (Fig. 5) are less than 0.5 m.

We make the following observations.

- *Low frequencies* ($0.6f_p$–$0.8f_p$): SWAN underpredicts spreading (bias of −24°) and there is much scatter [$\varepsilon_{\text{RMS}} = 27°$ and the scatter index (SI) = 0.52]. Note

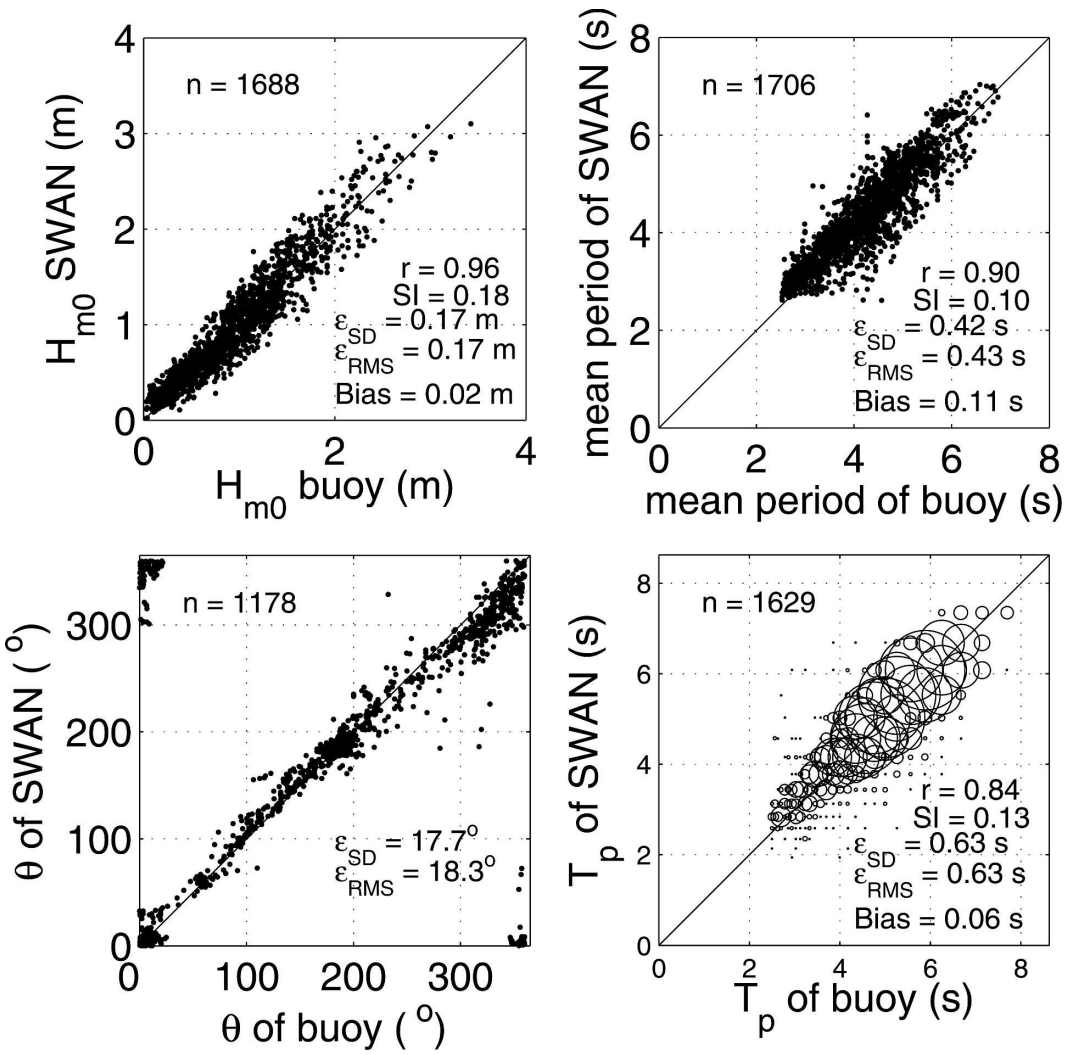

FIG. 5. Scatterplot comparison of wave height, mean period, true peak period, and mean–mean wave direction for the hindcast. The statistics listed are correlation coefficient (r), scatter index (SI), std dev of error (ε_{SD}), rms error (ε_{RMS}), and mean error (bias). In the plot of true peak period, points are not plotted; instead, the density of points is indicated by the size of the circles.

that in this case, even the mean value for the "ground truth" is not reliable; this is discussed in detail in section 6.

- *Frequencies near peak* ($0.8f_p$–$1.2f_p$): Random error is smaller ($\varepsilon_{RMS} = 6.5°$), but still not as good as it is for the other metrics (wave height, etc.). There is not a discernable systematic error (bias = 1.2°). The agreement is especially good for moderate and large wave heights (Fig. 6b). Note that the buoy data are more reliable for these moderate and large wave heights (Anctil et al. 1993).
- *Frequencies above the peak* ($1.2f_p$–$2f_p$): SWAN does not do a very good job of following the observations (predicted spreading varies much less than the observed spreading, $r = 0.44$), but error tends to be low[4] ($\varepsilon_{RMS} = 5.6°$), and there is no significant systematic error (bias = 2°).
- *Highest frequencies* ($2f_p$–$3f_p$): Like the prior frequency range, SWAN does not do a very good job of following the observations ($r = 0.44$): predicted spreading is consistently close to 40°. However, again the error tends to be low ($\varepsilon_{RMS} = 4.5°$), since the

[4] Judgment of what constitutes "low" rms error in directional spreading is necessarily subjective; it can be compared with expected measurement uncertainty. For substantiation—why this level of random error might be considered "low"—see section 6.

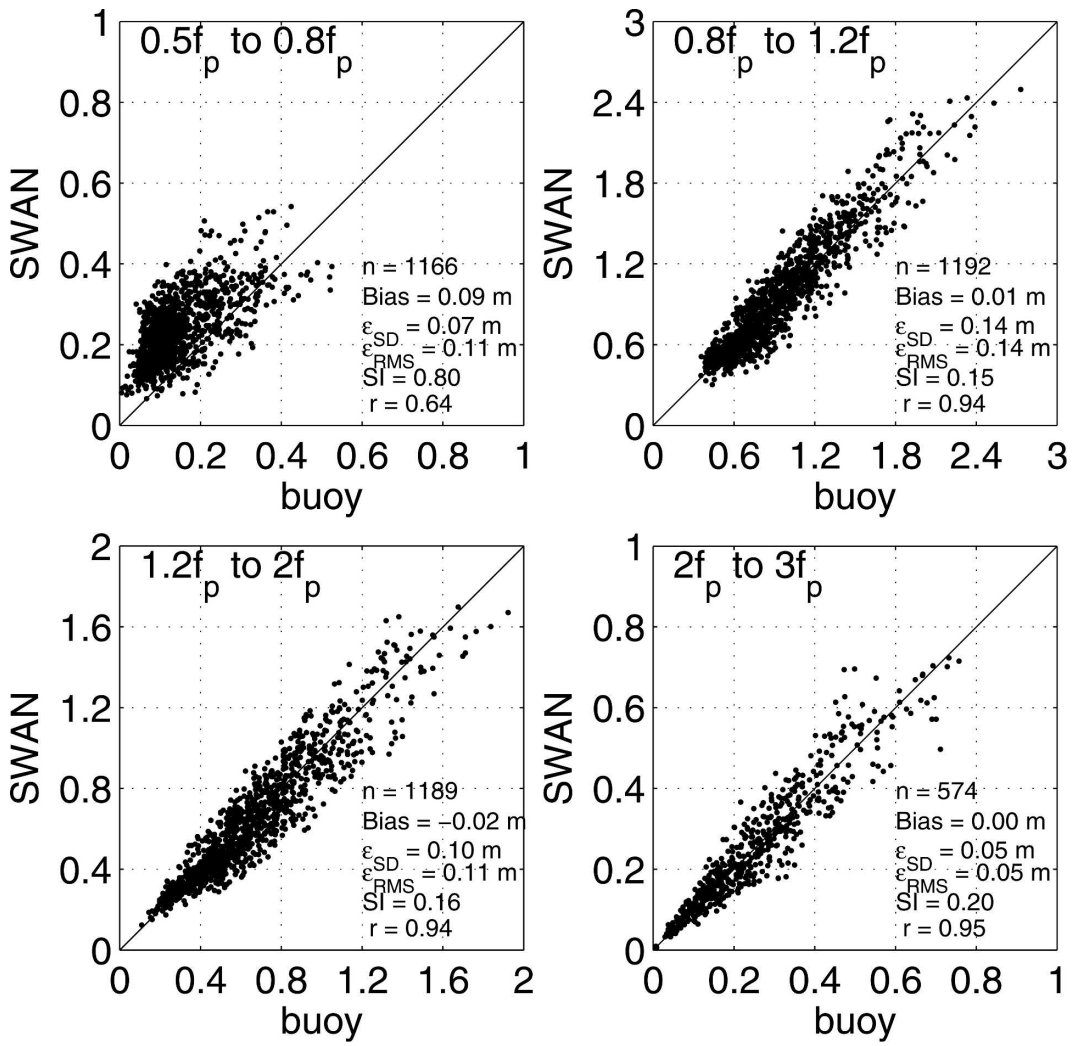

FIG. 6. Comparison of "partial wave height" (m), describing the energy level in the four frequency bands described in section 2.

observations, though they show more variation, are also clustered near 40°.

(ii) Time-averaged comparisons

To perform time averaging, the hindcast and observed directional spreading are calculated over smaller frequency bins of $0.1f_p$ (so the bins are $0.5f_p$, $0.6f_p$, . . . , 2.7 f_p, $2.8f_p$). To enhance stability, the integration to calculate $\overline{\sigma}_\theta$ is performed over a $\pm 0.1\, f_p$ range, so points are used more than once, similar to a moving average comparison. A simple time averaging is used (i.e., the values are not weighted). The resulting distributions are shown in Fig. 9, along with the empirical parametric model of Donelan et al. (1985), which was extended by Banner (1990) [see also Young (1999), Eq. (5.66)].

At the lower frequencies, directional spreading of the buoy is approximately 60% higher than that of either the parametric model or the numerical model. At the highest frequencies, the directional spreading of the parametric model is approximately 25% higher than that of the buoy and the numerical model.

5. Summary of results regarding bias in directional spreading

Our reading of the literature—specifically, Khandekar et al. (1994), Forristall and Ewans (1998), Forristall and Greenwood (1998), Cardone and Resio (1998), Wyatt et al. (2003)—gave us the impression that third-generation wave models such as WAM have a fairly consistent tendency to overpredict directional spreading. In Forristall and Greenwood (1998) (and see also

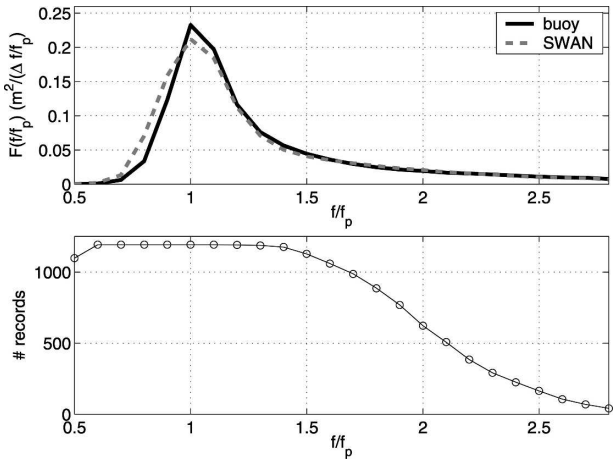

FIG. 7. (top) Time-averaged nondirectional spectrum $F(f/f_p)$. (bottom) Number of time records used to create a time average at each of the 24 f/f_p bins.

Cardone and Resio 1998), the problem is quite reasonably attributed to inaccuracy associated with the DIA approximation of nonlinear interactions used in third-generation wave models.

In this section we consider the results of the hindcast together with those of the idealized simulations and contrast both to our prior expectations. For the idealized simulations, a model with exact calculations of nonlinear interactions is taken as "ground truth" while for the hindcast, buoy data are taken as ground truth.

The comparison

Low frequencies: Our prior expectation was that the model directional distribution would be too broad, but in the long hindcast, the model directional spreading is narrow relative to the ground truth. In the idealized case the "model" is close to the ground truth (only slightly too narrow).

Near the peak: Our prior expectation was that the model directional distribution would be too broad, but in both the idealized case and the long hindcast, the average model directional spreading is quite close to that of the ground truth.

High frequencies: Our prior expectation was that the model directional distribution would be too broad. The idealized simulation supports this, but in the long hindcast, the average model directional spreading is quite close to that of the ground truth.

As a sort of a disclaimer, we refer above to other third-generation wave models used in prior studies. We do not imply that, had we used another 3G wave model in our hindcast, our results would be the same. We are contrasting our results with our prior expectations. Just as biases in predictions of nondirectional moments (e.g., wave height, mean period) are obviously sensitive to a model's source–sink formulations (wind input, dissipation, etc.), biases in predictions of directional width $\sigma_\theta(f)$ should be expected to be sensitive to these formulations.

6. Discussion

a. Accuracy of mean direction in turning winds

Comparisons of mean wave directions for this hindcast simulation show rather good accuracy overall. The response of a 3G wave model to rapidly turning winds is a concern. We do not specifically address this problem here, but we do not mean to imply that it is not an area in which the models may bear significant improvement.

b. Fetch geometry

The influence of the fetch geometry is represented within the formulation of third-generation wave models such as SWAN. Thus, it is presumed that the observed and modeled spectra are both influenced by the geometry of Lake Michigan. Ataktürk and Katsaros (1999, p. 643), cite a large reduction in wave energy—modeled and observed—associated with the narrow width of Lake Washington. Since it is a relatively large lake, this effect is expected to be much less pronounced in Lake Michigan, perhaps more comparable to the Lake Ontario observations cited in Ataktürk and Katsaros (1999), which are from Donelan et al. (1985).

c. The challenge of mixed seas and swells

In the case of mixed seas and swells, the challenge of directional validation is much greater. The location of our hindcast was deliberately chosen to avoid this additional complexity. Frequency-wise integration introduces the risk of mixing multiple components (e.g., seas and swells). A frequency-integrated metric (e.g., mean direction or directional spreading) that includes multiple wave systems is of dubious value. Under such circumstances, in order to present the type of comparison made here (e.g., in Figs. 6 and 7), the windsea component must be identified and separated from the swell components.

Methods for separating individual sea and swell components in a wave spectrum exist in the literature (e.g., Beal 1991; Gerling 1992; Komen et al. 1994; Hanson and Phillips 2001). Thus, it is theoretically possible to compare measured and observed wave spectra in a component-wise fashion (Hanson and Jensen 2004).

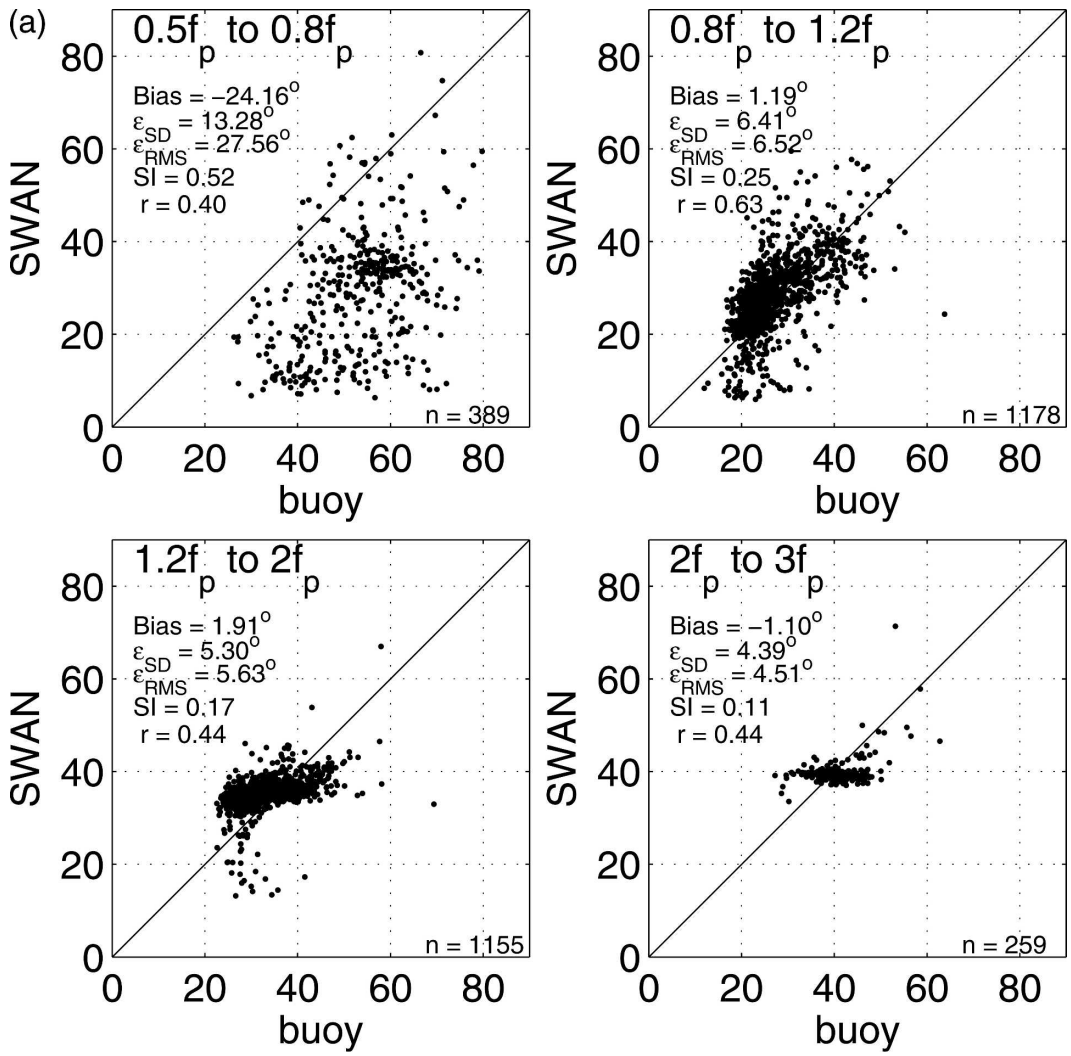

FIG. 8. (a) Scatterplot comparisons (hindcast vs observation) of mean directional spreading (°) over four frequency ranges. (b) Scatterplot comparisons (hindcast vs observation) for four frequency ranges. The horizontal axis is the buoy partial wave height for the indicated frequency range, and the vertical axis is the misfit in mean directional spreading (hindcast − observed).

Unfortunately, due to model limitations, it is not uncommon to have a swell system that exists in observations but not in the model spectra, or vice versa. In this case, validation of the directional spreading is obviously not possible.

Based on our experiences, we expect that a validation such as was performed here would be difficult for an exposed coastline, with frequent mixed sea–swell conditions. In such a case, some compromise is probably necessary. By way of summary, two possible compromises are to either

1) consider a shorter time period, so that qualitative comparisons can be made, for example by graphing $\sigma_\theta = \sigma_\theta(f, t)$ and $E = E(f, t)$, or
2) separate the windsea from swell components, and validate the directional spreading of the windsea component.

Of course, it is possible to evaluate the directional spreading of swell components also. This was done for observational data by Ewans (2001). However, if the objective is to evaluate generation-stage source–sink terms, study of the directional spreading of the windsea seems to be the most direct approach.

d. Sensitivity of results to method of calculation of peak frequency

It is well accepted (e.g., Donelan et al. 1985; Banner 1990) that a typical windsea directional distribution will

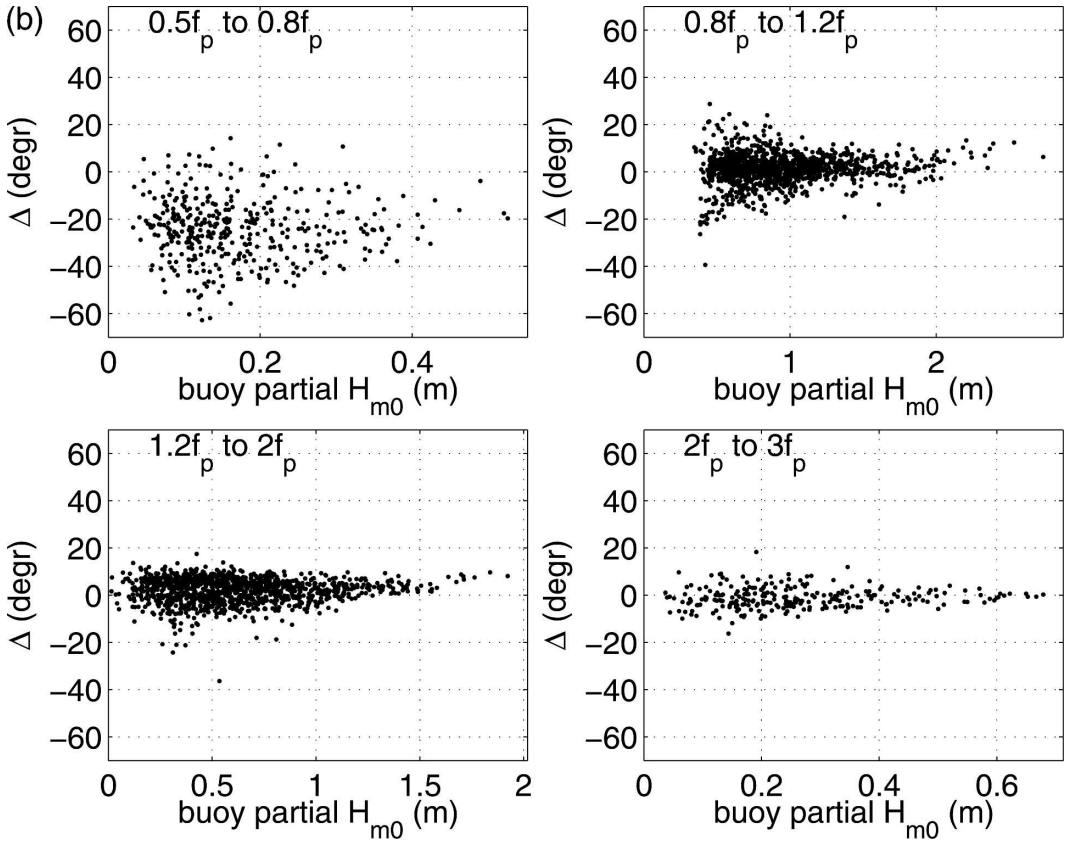

FIG. 8. (*Continued*)

tend to be most narrow somewhere near the peak frequency. The most natural way to analyze this behavior (or lack thereof) in a model and collocated observations is via normalization of the results by peak frequency, as is done here. However, this does introduce some ambiguity. There are multiple options regarding which peak frequency to use (model peak, buoy peak, or some combination), and one can expect that results will demonstrate some sensitivity to this choice unless fairly broad frequency bands (e.g., the four bands used in Figs. 6 and 8) are used. With small frequency bands very near the spectral peak (say, 0.95–1.05 f_p), one should not be surprised if even the sign of the bias is not robust. Thus, it is critical to use consistent methods when intercomparing statistics from different hindcasts.

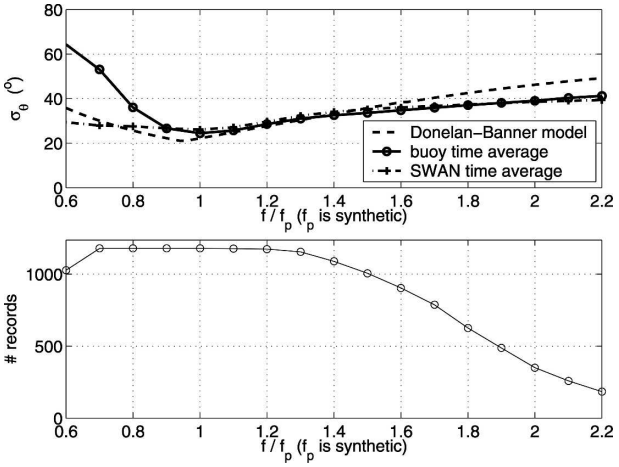

FIG. 9. Comparison of time-averaged results (model and observation) with the parametric model of Donelan et al. (1985) and Banner (1990). The bottom panel shows the number of time records used to create a time average for the model and buoy data at each of the 17 f/f_p bins.

e. Consideration of uncertainty in observations

It is useful to put the model–data misfit in the context of measurement error. Quoting Voorips et al. (1997), "Observation errors consist of instrumental errors, errors due to the random variability of the spectrum and limited sample time, and representation errors. Representation error is the difference between what the buoy actually measures . . . . and its model equivalent." Statistical error—determined by degrees of freedom—has been successfully incorporated into a validation of non-

directional spectra by Alves et al. (2002). Unfortunately, no such method exists that accounts for the total error, since this is not defined, at least not in the context of spectral density from 3-m discus buoys.

Kuik et al. (1988) estimate the confidence limits on directional moments based on statistical uncertainty; in terms of rms error, they are 5°–10° for mean direction, 10%–15% for directional width, 30%–50% for skewness, and 25%–100% for kurtosis (see also Anctil et al. 1993). So, 0.10–0.15 can be compared with the scatter index values given in Fig. 8a.

Measurement of long, low-amplitude waves by buoys is problematic due to the weak acceleration or slope signal against the background noise. However, we do not know of any arguments that this may manifest itself as *bias* in the spectral density. In contrast, it has been shown by Kuik et al. (1988) that low levels of noise in the surface elevation or slope will cause a positive bias in the directional spread (see also discussions in O'Reilly et al. 1996). In the case of the low frequencies, the directional spreading of the buoy used as ground truth in the hindcast herein is almost certainly too high. This behavior is consistent with the overestimating of the directional spreading of swells by NDBC 3-m discuss buoys, as reported by O'Reilly et al. (1996) (a 6° bias, with the metric integrated over 0.06–0.14 Hz).

To summarize, in the model–buoy comparisons herein, bias below the spectral peak is evident both in the spectral density $F(f)$ and the directional spread $\sigma_\theta(f)$. Bias in $\sigma_\theta(f)$ below the peak cannot be definitively attributed to the model, whereas bias in $F(f)$ below the peak is credibly attributed to the model.

f. The high-frequency cutoff in the idealized simulations

The WAVEWATCH-III and WAM models employ a diagnostic tail above a prescribed frequency relative to the spectral peak frequency. Banner and Young (1994) point out that removal of this tail has dramatic consequences on all quantities derived from the wave spectrum. SWAN, however does not employ a self-adjusting high-frequency cutoff, and in the idealized simulations herein, we use a high frequency cutoff fixed at 1.0 Hz, which is in fact higher than the fixed cutoff frequency used by Banner and Young (1994). Thus, there is less concern about the effect of the parametric tail on the results presented. However, these same simulations were performed with the WAVEWATCH-III model (not shown herein), and the qualitative impact of the nonlinear solver, WRT versus DIA, in this simulation is similar regardless of which model is used as the platform.

g. The impact of the nonlinear solver in a hindcast

Though we apply the WRT nonlinear solver in an idealized scenario, it would be possible to apply it in a shortened version of our Lake Michigan hindcast to specifically study the impact of the inaccuracy of the DIA. Presuming that the WRT-based model would have narrower spreading in high frequencies (vs. the DIA-based model), we can reasonably expect that the WRT-based method would *underpredict* the directional spreading in the high frequencies in this hindcast. Obviously, this indicates a situation in which a model (the DIA-based model) is correct for the wrong reasons. Indeed, if this pattern is systematic (observed in other hindcasts), it would justify a retuning of the directional spreading of the wind input term in SWAN to create broader directional spreading in the high frequencies with the WRT-based model. We believe that in any case, a move to more accurate calculations of nonlinear interactions will necessitate retuning of the other two deepwater source–sink terms.

In fact, a hindcast with a WRT-based model has been performed recently (F. Ardhuin 2005, personal communication), which suggests that DIA does lead to broader directional spectra in the higher frequencies, compared to a model with exact nonlinear computations. With the WAM3 physics (also employed in the present study), the DIA-based model tends to be too broad overall and the WRT-based model tends to be too narrow, in the higher frequencies, compared to observations. Further, an interesting question is raised by the authors of that study: whether modeled directional spreading is sensitive to directional spreading of the S_{in} term, or controlled solely by the S_{nl4} term. Further, our experience is that modeled directional spreading is sensitive to the S_{ds} term: we have verified that our a priori choice of the weighting on the relative wavenumber in S_{ds} (section 4a) *does* affect the bias statistics presented in Fig. 8. Arguments exist in the literature that high-frequency directional spreading *in nature* is controlled solely by the S_{nl4} term (Young and Van Vledder 1993; Banner and Young 1994; Young et al. 1995).

h. Potential subsequent work

A subsequent, more ambitious directional validation exercise might be of longer duration, with multiple observational points, and might also consider higher-order moments: skewness and kurtosis.

7. Conclusions

In an enclosed basin such as Lake Michigan, it is demonstrated herein that it is possible to quantitatively

validate directional characteristics—mean direction and directional spreading—of a relatively long wave model hindcast. Further, buoy observations can be used in such a validation without applying a parametric model (such as the $\cos^{2s}$ model) or a data-adaptive method (such as the MLE or MEM) to the observations. Populations of model–observation pairs such as the scatterplot comparisons herein are readily condensed to statistics such as root-mean-square error, bias, and standard deviation of error, so it is feasible to present directional validations for multiple locations within limited space, such as a journal article.

Due to the considerable added complexity associated with mixed sea–swell conditions, it is not as straightforward to perform a validation in this manner on an exposed coastline. Some sea–swell separation algorithm would need to be applied.

In addition to the validation of the long hindcast, a pair of idealized simulations is presented herein to aid in the interpretation of the results. The two idealized simulations differ in their methods of calculating the nonlinear interaction [essentially an exact method (WRT) versus an operational method (DIA)]. Considering both the hindcast validation and the idealized simulations, we find the following about the bias characteristics.

- At frequencies below the spectral peak, in both the idealized case and the long hindcast, the model directional spreading is narrow relative to the ground truth. In the case of the hindcast, however, the signal-to-noise ratio of the ground truth may be poor at these low frequencies. In the example of the idealized case, the bias is very slight. In both cases, model energy is overpredicted in this frequency range, limiting the validity of the comparison of the directional spreading.
- Near the peak frequency, in both the idealized case and the long hindcast, the average model directional spreading is quite close to that of the ground truth.
- At frequencies above the spectral peak, the model in the idealized simulation is too broad relative to the ground truth, but in the long hindcast, the average model directional spreading is quite close to that of the ground truth.

Regarding statistics other than bias, in the long hindcast at all frequency bands, model–data agreement is not favorable except in high-energy conditions.

Acknowledgments. This work was supported by the Office of Naval Research through the 6.1 Naval Research Laboratory project: Transient Development of Nonlinear Wind-Generated Ocean Waves. Unpublished work by Dr. W. C. O'Reilly (Scripps Institution of Oceanography) influenced the methodology used in this paper. We acknowledge discussions with Dr. Fabrice Ardhuin (Centre Militaire d'Oceanographie) and Dr. Robert Jensen (Army Corps of Engineers) during the preparation of this manuscript. We also thank Dr. Ardhuin for providing an early version of his manuscript. This paper has been approved for public release by the Naval Research Library. The National Centers for Environmental Prediction (NCEP) technical notes are not formally published, but electronic versions are available online from the NCEP Web site www.ncep.noaa.gov.

REFERENCES

Alves, J. H. G. M., D. J. M. Greenslade, and M. L. Banner, 2002: Impact of a saturation-dependent dissipation source function on operational hindcasts of wind-waves in the Australian region. *Global Atmos. Oceanic Syst.,* **8,** 239–267.

——, and M. L. Banner, 2003: Performance of a saturation-based dissipation-rate source term in modeling the fetch-limited evolution of wind waves. *J. Phys. Oceanogr.,* **33,** 1274–1298.

Anctil, F., M. A. Donelan, G. Z. Forristall, K. E. Steele, and Y. Ouellet, 1993: Deep-water field evaluation of the NDBC-SWADE 3-m discus directional buoy. *J. Atmos. Oceanic Technol.,* **10,** 97–112.

Ardhuin, F., W. C. O'Reilly, T. H. C. Herbers, and P. F. Jessen, 2003: Swell transformation across the continental shelf. Part I: Attenuation and directional broadening. *J. Phys. Oceanogr.,* **33,** 1921–1939.

Ataktürk, S. S., and K. B. Katsaros, 1999: Wind stress and surface waves observed on Lake Washington. *J. Phys. Oceanogr.,* **29,** 633–650.

Banner, M. L., 1990: Equilibrium spectra of wind waves. *J. Phys. Oceanogr.,* **20,** 966–984.

——, and I. R. Young, 1994: Modeling spectral dissipation in the evolution of wind waves. Part I: Assessment of existing model performance. *J. Phys. Oceanogr.,* **24,** 1550–1571.

Beal, R. C., Ed., 1991: *Directional Ocean Wave Spectra*. The Johns Hopkins University Press, 218 pp.

Benoit, M., P. Frigaard, and H. A. Schäffer, 1997: Analysing multidirectional wave spectra: A tentative classification of available methods. *Proc. Int. Association of Hydraulic Engineering and Research: Multidirectional Waves and Their Interaction with Structures,* San Francisco, CA, National Research Council of Canada, 131–157.

Booij, N., R. C. Ris, and L. H. Holthuijsen, 1999: A third-generation wave model for coastal regions, 1, Model description and validation. *J. Geophys. Res.,* **104,** 7649–7666.

——, I. J. G. Haagsma, L. H. Holthuijsen, A. T. M. M. Kieftenburg, R. C. Ris, A. J. van der Westhuysen, and M. Zijlema, 2005: SWAN Cycle III, version 40.41. User manual, Delft University of Technology, Delft, the Netherlands, 115 pp. [Available online at http://fluidmechanics.tudelft.nl/swan/index.htm.]

Capon, J., R. J. Greenfield, and R. J. Kolker, 1967: Multidimensional maximum-likelihood processing of a large aperture seismic array. *Proc. IEEE,* **55,** 192–211.

Cardone, V. J., and D. T. Resio, 1998: An assessment of wave

modeling technology. *Proc. Fifth Int. Workshop on Wave Hindcasting and Forecasting,* Melbourne, FL, Environment Canada, 468–495.

Cartwright, D. E., 1963: The use of directional spectra in studying the output of a wave recorder on a moving ship. *Conference on Ocean Wave Spectra,* Prentice Hall, 203–218.

Donelan, M. A., J. Hamilton, and W. H. Hui, 1985: Directional spectra of wind-generated waves. *Philos. Trans. Roy. Soc. London,* **315A,** 509–562.

Ewans, K. C., 2001: Directional spreading in ocean swell. *Proc. Int. Symp. on Ocean Wave Measurement and Analysis,* San Francisco, CA, American Society of Civil Engineers, 517–529.

Ewing, J. A., and A. K. Laing, 1987: Directional spectra of seas near full development. *J. Phys. Oceanogr.,* **17,** 1696–1706.

Forristall, G. Z., and K. C. Ewans, 1998: Worldwide measurements of directional wave spreading. *J. Atmos. Oceanic Technol.,* **15,** 440–469.

——, and J. A. Greenwood, 1998: Directional spreading of measured and hindcasted wave spectra. *Proc. Fifth Int. Workshop on Wave Hindcasting and Forecasting,* Melbourne, FL, Environment Canada, P5–P15.

——, E. G. Ward, V. J. Cardone, and L. E. Borgmann, 1978: The directional spectra and kinematics of surface gravity waves in Tropical Storm Delia. *J. Phys. Oceanogr.,* **8,** 888–909.

Gerling, T. W., 1992: Partitioning sequences and arrays of directional wave spectra into component wave systems. *J. Atmos. Oceanic Technol.,* **9,** 444–458.

Hanson, J. L., and O. M. Phillips, 2001: Automated analysis of ocean surface directional wave spectra. *J. Atmos. Oceanic Technol.,* **18,** 277–293.

——, and R. E. Jensen, 2004: Wave system diagnostics for numerical wave models. *Proc. Eighth Int. Workshop on Wave Hindcasting and Forecasting,* North Shore, Oahu, HI, Environment Canada, Paper E3. [Available online at http://www.waveworkshop.org/8thWaves/Papers/E3.pdf.]

Hasselmann, S., K. Hasselmann, J. H. Allender, and T. P. Barnett, 1985: Computations and parameterizations of the nonlinear energy transfer in a gravity-wave spectrum. Part II: Parameterizations of the nonlinear energy transfer for application in wave models. *J. Phys. Oceanogr.,* **15,** 1378–1391.

Jensen, R. E., C. M. Holmes, and C. L. Dorion, 1995: An evaluation of two extreme storm events in the mid-Atlantic coastal waters: measurement and 3GWAM assessment. *Proc. Fourth Int. Workshop on Wave Hindcasting and Forecasting,* Banff, AB, Canada, Environment Canada, 235–249.

Khandekar, M. L., R. Lalbeharry, and V. Cardone, 1994: The performance of the Canadian Spectral Ocean Wave Model (SSOWM) during the Grand Banks *ERS-1* SAR wave spectra validation experiment. *Atmos.–Ocean,* **32,** 31–60.

Komen, G. J., S. Hasselmann, and K. Hasselmann, 1984: On the existence of a fully developed wind-sea spectrum. *J. Phys. Oceanogr.,* **14,** 1271–1285.

——, L. Cavaleri, M. Donelan, K. Hasselmann, S. Hasselmann, and P. A. E. M. Janssen, 1994: *Dynamics and Modelling of Ocean Waves.* Cambridge University Press, 532 pp.

Kuik, A. J., G. van Vledder, and L. H. Holthuijsen, 1988: A method for the routine analysis of pitch-and-roll buoy wave data. *J. Phys. Oceanogr.,* **18,** 1020–1034.

Longuet-Higgins, M. S., D. E. Cartwright, and N. D. Smith, 1963: Observations of the directional spectrum of sea waves using the motions of a floating buoy. *Conference on Ocean Wave Spectra,* Ed., Prentice Hall, 111–136.

Lygre, A., and H. E. Krogstad, 1986: Maximum entropy estimation of the directional distribution in ocean wave spectra. *J. Phys. Oceanogr.,* **16,** 2052–2060.

Oltman-Shay, J., and R. T. Guza, 1984: A data-adaptive ocean wave directional-spectrum estimator for pitch and roll type measurements. *J. Phys. Oceanogr.,* **14,** 1800–1810.

O'Reilly, W. C., T. H. C. Herbers, R. J. Seymour, and R. T. Guza, 1996: A comparison of directional buoy and fixed platform measurements of Pacific swell. *J. Atmos. Oceanic Technol.,* **13,** 231–238.

Resio, D. T., and W. Perrie, 1991: A numerical study of nonlinear energy fluxes due to wave–wave interactions, I, Methodology and basic results. *J. Fluid Mech.,* **223,** 609–629.

Rogers, W. E., and D. W. C. Wang, 2006: On the validation of directional wave prediction: Review and discussion. NRL Memo. Rep., NRL/MR17320-06-8970, 40 pp.

——, P. A. Hwang, and D. W. Wang, 2003: Investigation of wave growth and decay in the SWAN model: Three regional-scale applications. *J. Phys. Oceanogr.,* **33,** 366–389.

Steele, K. E., J. C. Lau, and Y. L. Hsu, 1985: Theory and application of calibration techniques for an NDBC directional wave measurements buoy. *IEEE J. Oceanic Eng.,* **10,** 382–396.

Tolman, H. L., 1991: A third-generation model for wind waves on slowly varying, unsteady, and inhomogeneous depths and currents. *J. Phys. Oceanogr.,* **21,** 782–797.

——, 2002: User manual and system documentation of WAVEWATCH-III Version 2.22. NCEP Tech. Note 222, 133 pp. [Available online at www.ncep.noaa.gov.]

——, and D. Chalikov, 1996: Source terms in a third-generation wind wave model. *J. Phys. Oceanogr.,* **26,** 2497–2518.

Voorips, A. C., V. K. Makin, and S. Hasselmann, 1997: Assimilation of wave spectra at pitch-and-roll buoys in a North Sea wave model. *J. Geophys. Res.,* **102,** 5829–5849.

WAMDI Group, 1988: The WAM model—A third generation ocean wave prediction model. *J. Phys. Oceanogr.,* **18,** 1775–1810.

Wyatt, L. R., and Coauthors, 2003: Validation and intercomparisons of wave measurements and models during the EuroROSE experiments. *Coastal Eng.,* **48,** 1–28.

Young, I. R., 1994: On the measurement of directional wave spectra. *Appl. Ocean Res.,* **16,** 283–294.

——, 1999: *Wind Generated Ocean Waves.* Elsevier, 288 pp.

——, and G. Ph. Van Vledder, 1993: A review of the central role of nonlinear interactions in wind-wave evolution. *Philos. Trans. Roy Soc. London,* **342A,** 505–524.

——, S. Hasselmann, and K. Hasselmann, 1987: Computations of the response of a wave spectrum to a sudden change in wind direction. *J. Phys. Oceanogr.,* **17,** 1317–1338.

——, L. A. Verhagen, and M. L. Banner, 1995: A note on the bimodal directional spreading of fetch-limited waves. *J. Geophys. Res.,* **100,** 773–778.